Comparative metabolomics with Metaboseek reveals functions of a conserved fat metabolism pathway in *C. elegans*

Maximilian J. Helf[1,#], Bennett W. Fox[1,#], Alexander B. Artyukhin[2], Ying K. Zhang[1], Frank C. Schroeder[1,*]

[1]Boyce Thompson Institute and Department of Chemistry and Chemical Biology, Cornell University, Ithaca, New York 14853, United States

[2]Chemistry Department, College of Environmental Science and Forestry, State University of New York, Syracuse, New York 13210, United States

[#]These authors contributed equally to this work

*Correspondence to fs31@cornell.edu

ABSTRACT

Untargeted metabolomics via mass spectrometry (MS) can reveal several 100,000 molecular features in a single sample, most of which may represent unidentified metabolites, posing significant challenges to data analysis. We here introduce Metaboseek, an open-source analysis platform designed for untargeted comparative metabolomics, and demonstrate its utility to elucidate functions of a conserved fat metabolism pathway, α-oxidation, using *C. elegans* as a model. Metaboseek integrates modules for molecular feature detection, statistics, molecular formula prediction, and MS/MS analysis, which uncovered more than >200 previously uncharacterized α-oxidation-dependent metabolites in an untargeted comparison of wildtype and α-oxidation-defective *hacl-1* mutants. The identified structures support the predicted enzymatic function of HACL-1 and revealed that α-oxidation participates in metabolism of endogenous β-methyl-branched fatty acids and food-derived cyclopropane lipids. Our results showcase compound discovery via untargeted comparative metabolomics applied to a conserved primary metabolic pathway and suggest a model for the metabolism of cyclopropane lipids that are also part of human diets.

MAIN

Widespread adoption of high-resolution mass spectrometry (HRMS) for untargeted metabolomics has revealed a vast universe of biogenic small molecules, including a large number of compounds whose chemical structures have not been elucidated ("unknowns")[1]. Many of these metabolites may serve important biological functions, as intra- or intercellular signaling molecules, e.g., as hormones, or mediating communication at the inter-organismal level, e.g., in host-microbe interactions or as pheromones[2–5]. Their large-scale identification, quantitation, and elucidation of underlying biosynthetic networks promises to advance mechanistic understanding of phenotypes and complement transcriptomics and proteomics[6–9].

However, the highly irregular and often unpredictable structures of metabolites pose a largely unmet challenge to their systematic chemical and biological annotation. HPLC-HRMS analysis of a typical metabolome sample of plant or animal origin can reveal several 100,000 molecular features (defined by a mass-to-charge ratio, *m/z*, and retention time, RT), most of which may represent compounds whose structures are unknown[9–11]. Comparative analyses of metabolome samples representing different biological conditions or genetic backgrounds are

then used to identify features that are significantly differential between conditions, akin to finding induced or repressed genes in transcriptomics. In the case of untargeted metabolomics, such comparative analyses provide the basis for prioritizing among the many detected unknowns for subsequent structure elucidation[12], which is often time- and resource-intensive.

Processing of metabolomics data involves three major steps, each of which comes with its own challenges and open-source computational tools: (i) feature detection, e.g., using xcms[13,14], mzMine[15], MS-DIAL[16,17], (ii) comparative statistical analysis, e.g., MetaboAnalyst[18], xcms online[19], and (iii) structural characterization, e.g., MS FINDER[20], CFM-ID[21], SIRIUS[22]. Online resources such as GNPS provide access to vast amounts of MS data, with growing support for data browsing that highlights the demand for facilitated access to the raw data from metabolomics studies[23,24]. Importantly, comparative metabolomics requires effective, multi-layered interaction with MS and MS/MS data to enable annotation and prioritization of differentially regulated molecular features, in particular when the analyses are truly untargeted and focused on the identification of unknowns. Exploring the metabolomes of *C. elegans* and other model systems, we recognized the need for an open-source analysis platform that can serve as a flexible and customizable hub integrating diverse existing tools.

We here introduce *Metaboseek*, a modular software platform that provides a comprehensive data analysis workflow, from feature detection to compound identification, specifically designed to facilitate untargeted metabolomics. Metaboseek incorporates popular metabolomics tools and makes them available in an intuitive, browser-based graphical user interface (**Figure 1**). In addition Metaboseek facilitates the validation of results from computational analyses, such as differential molecular features detected by xcms[14] or adduct assignments by CAMERA[25] via extensive filtering options. Compound identification is supported by built-in MS/MS molecular networking capabilities and a module that interacts with the SIRIUS software for MS/MS fragment annotation and metabolite identification with CSI:FingerID[22].

We then leverage Metaboseek to investigate peroxisomal α-oxidation (pαo) in *C. elegans*, a conserved fatty acid degradation pathway that functions in parallel with β-oxidation and is required for the metabolism of β-branched fatty acids. Whereas β-oxidation takes place in both mitochondria and peroxisomes, α-oxidation occurs exclusively in peroxisomes, which are membrane-bound metabolic compartments that function coordinately with other organelles in lipid and bile acid metabolism[26]. Previous unbiased comparative analysis of a mutant defective in peroxisomal β-oxidation (*daf-22*) and wildtype (WT) *C. elegans* revealed a family of

glycolipids, the ascarosides[27], which play a central role in *C. elegans* biology[28]. In contrast to peroxisomal β-oxidation, the pαo pathway in *C. elegans* has not been investigated. Using Metaboseek for untargeted comparative metabolomics of a pαo mutant, we show that disruption of *C. elegans* pαo results in accumulation of several 100 metabolites, most of which have not previously been reported. The identified metabolites support homology-based annotation of pαo pathway enzymes and indicate a role for pαo in the processing food-derived cyclopropane fatty acids, which are also part of human diets.

RESULTS

The Metaboseek workflow. In a typical metabolomics workflow, HPLC-HRMS and MS/MS data acquisition is followed by *Feature Detection* (a "feature" representing a specific *m/z*, RT pair) and *Feature Grouping* (aiming to recognize the same features across different samples, a non-trivial step, especially in the case of closely eluting isomers). Metaboseek integrates the *xcms* package for feature detection and grouping, generating a feature table containing the data for all identified molecular features, including *m/*z range, RT range, and intensity values for a given feature in each sample. Alternatively, feature tables can be imported from external tools, such as mzMine, MS-DIAL, or xcmsOnline. Following feature detection and grouping, any subsequent statistical or data-dependent analysis generates new columns in the *Feature Table*, which serves as a customizable information hub that guides data analysis.

The *Data Explorer* section is at the heart of Metaboseek, providing the platform to further process, prioritize, sort, and visualize molecular features within the feature table. An extensive range of filters can be used in any user-defined configuration to enable robust prioritization and intuitive sorting of features, e.g., mean intensity threshold and fold change of a feature between different sample groups, at a specific significance level. Finding molecular features with significantly differential abundances in Metaboseek is assisted by built-in *t*-test and ANOVA, as well as group-wise fold-change metrics. For more advanced statistical analysis, feature tables can be exported directly in a MetaboAnalyst-compatible format[18]. Features of interest can be manually inspected in the interactive user interface, which includes a customizable *Data Viewer* for visual validation of molecular features, modules for *Molecular Formula Prediction* and isotope/adduct assignments, and interactive *MS/MS Molecular Networking*. MS/MS spectra can be easily compared to each other or annotated using SIRIUS fragmentation trees and CSI:FingerID database matching[21,22]. The Metaboseek *Data Explorer* further incorporates an isotope tracing module, *Label Finder*, providing an integrated analysis option for stable isotope

labeling experiments (**Figure 1**). Like many popular open-source MS data analysis tools, Metaboseek is written in R, using the *shiny* R package for interactive data visualization, and thus can be run either on a server or locally on any computer. All data analysis steps are tracked so that settings can be archived and reproduced. Extensive documentation for Metaboseek is available online.

Citronellic acid as a probe for α-oxidation. A putative *C. elegans* α-oxidation pathway was proposed more than two decades ago, based on sequence similarity to characterized rat and human enzymes (**Figure 2A**)[29]. In humans, the principal function of α-oxidation is presumed to be the enzymatic digestion of β-branched fatty acids (**1**), such as (*R*)-citronellic acid (CA, **6**) (**Figure 2C**), which cannot be processed by β-oxidation[30]. In the first step of the human α-oxidation pathway, fatty acyl-coenzyme A (CoA) derivatives (**2**) are *syn*-hydroxylated at the α-position by the phytanoyl-CoA dioxygenase, PHYH, an iron-coordinating dioxygenase that is 52% and 59% similar to the uncharacterized *C. elegans* proteins, ZK550.5 and ZK550.6, respectively (**Figure 2A**)[31]. Genetic mutations in *PHYH* cause Refsum's syndrome, which is characterized by toxic accumulation of branched fatty acids in the blood and nervous system[32]. The next step is catalyzed by 2-hydroxyacyl-CoA lyase, HACL1, which binds thiamine pyrophosphate (TPP) as a cofactor and cleaves a C-C bond in the α-hydroxy, β-methylacyl-CoA (**3**) to produce formyl-CoA and an α-methyl fatty aldehyde (**4**). The aldehyde is then oxidized in an NAD^+-dependent reaction to the corresponding α-methyl fatty acid (**5**), which now is a suitable substrate for further processing via β-oxidation (**Figure 2A**).

To probe pαo in *C. elegans*, we compared metabolism of supplemented CA (**6**, **Figure 2B**) in WT animals and null mutants of *hacl-1*, the presumed homolog of human *HACL1*[29]. If *hacl-1* were required for α-oxidation, supplementation with CA should result in accumulation of an α-hydroxyl CA derivative (**7**), whose MS/MS spectrum should show a characteristic neutral loss of formic acid (**Figure 2C**)[33]. The custom filtering options and extracted ion chromatogram (EIC) display in Metaboseek facilitated screening molecular ions at the expected *m/z* of **7** (*m/z* 185.1183, $C_{10}H_{17}O_3^-$) that produce neutral loss of formic acid during MS/MS and were strongly enriched in *hacl-1* samples (**Figure 2D**). Of six other CA-derived features detected at *m/z* 185.1183, none were enriched in *hacl-1* relative to WT, nor did these features exhibit neutral loss of formic acid in MS/MS, suggesting these features are derived from hydroxylation of CA via other metabolic pathways (**Supplementary Figure 1**).

Additional CA-dependent features enriched in *hacl-1* relative to CA-supplemented WT animals were uncovered using a combination of fold change, intensity, and CA-supplementation dependent filters, which, after removal of adducts, revealed 32 CA-derived metabolites (**Supplementary Figure 1**). These differential features included multiply oxygenated CA derivatives, which could be ostensibly derived from ω-oxidation following stalled α-oxidation[34]. For example, we detected several features at *m/z* 201.1132 that elute over a wide RT range, representing dihydroxylated CA derivatives, two of which were *hacl-1*-enriched (such as **8**, see also **Supplementary Figure 1**). Additional *hacl-1*-dependent CA-derivatives included putative ethanolamides (**9**), glycosides (**10**), and an *N*-acyl glycerophosphoethanolamide conjugate (**Supplementary Figure 1**). For most of these compounds, MS/MS fragmentation between the α- and carbonyl carbons suggested α-hydroxylation of the citronellyl moiety (**Figure 2C**). Similar results were obtained when *hacl-1* worms were supplemented with geranic or phytanic acid (data not shown). Taken together, this supplementation study revealed a set of *hacl-1*-dependent shunt metabolites of CA, consistent with the proposed function of HACL-1 as a 2-hydroxyacyl-CoA lyase.

Endogenous C_{11} fatty acids enriched in *hacl-1* larvae. We next investigated the impact of *hacl-1* inactivation on endogenous metabolites, using molecular networking of MS/MS spectra acquired as part of in-depth untargeted HPLC-HRMS analysis of *hacl-1* mutants and WT *C. elegans*. The *Molecular Networking* tool in Metaboseek uses the feature grouping information from *xcms* to match MS/MS spectra with a corresponding molecular feature. Similarity scores are based on peak matching between pairs of averaged spectra, and subsequent calculation of the cosine score between relative peak intensities of the matched spectra, similar to the GNPS feature-based networking workflow[35]. The resulting networks can be easily viewed and evaluated in Metaboseek, which allows users to click nodes and compare MS/MS fragmentation patterns directly. Any information in the feature table, e.g., relative abundances of compounds across sample groups, comments, or statistical analyses, can be mapped onto the network view.

To assess the role of *hacl-1* in *C. elegans* metabolism, we initially focused on starved animals at the first larval stage (L1), a condition that allows the study of *C. elegans* metabolism in the absence of bacterial food[36]. Comparative analysis of negative ion MS data for L1 larvae revealed a small set of features strongly enriched in *hacl-1* relative to WT, several of which clustered together in the MS/MS network (**Figure 3A**). Stringent fold change (10-fold), intensity (top 1.25% of detected features), and unadjusted significance ($p < 0.05$) thresholds yielded 57

molecular features that were highly enriched in *hacl-1* larvae. Following *CAMERA* isotope/adduct assignment and manual curation, we detected 14 *hacl-1*-dependent metabolites (**Figure 3B**). Intriguingly, the majority of these compounds appeared to represent C_{11} fatty acids, based on their ionization properties and MS/MS spectra. Furthermore, MS/MS spectra of the most abundant *hacl-1*-enriched metabolites featured a glyoxylate ion at *m/z* 72.993 ($C_2HO_3^-$), which was not observed in any CA-derived metabolites (**Figure 3C**).

We selected one highly abundant *hacl-1*-enriched metabolite ($C_{11}H_{19}O_4^-$) for isolation by preparative HPLC followed by structure elucidation via 2D NMR spectroscopy (**Supplementary Figure 2** and **Supplementary Table S1**), which revealed an unusual β-methyl substituted, eleven-carbon fatty acid, named bemeth#3 (**11**, **Figure 3C**). α-Hydroxylation and the position of the double bond in bemeth#3 are consistent with the strong glyoxylate fragment ion in its MS/MS spectrum. Moreover, the structure of bemeth#3 suggested that other glyoxylate ion-producing metabolites that accumulate in *hacl-1* mutants also represent derivatives of α-hydroxylated β-methyl-4-decenoic acid (e.g., **12**, **Figure 3C**). These assignments were further supported via synthesis of an authentic sample of the two diastereomers of **12** (**Figure 3D**), whose MS/MS spectra and retention times were identical to those of the corresponding *hacl-1*-enriched metabolites (**Figure 3E**). Other metabolites enriched in *hacl-1* include less abundant isomers of **11** and **12** with identical MS/MS fragmentation, as well as derivatives that appear to have undergone additional oxidation, including putative dicarboxylic acids, such as $C_{11}H_{17}O_5^-$ (**Supplementary Figure 3**). Taken together, analysis of *hacl-1* larvae revealed an unusual family of C_{11} fatty acids based on the β-methyl-decenoic acid scaffold, which has not previously been reported from animals. α-Hydroxylation in the identified C_{11} acids **11** and **12** suggests that they represent substrates of HACL-1 that accumulate due to stalled pαo in *hacl-1* mutants. The additional dihydroxylated and diacid-derivatives could results from subsequent ω- and (ω-1)-oxidation of **12**, as part of a "rescue pathway," similar to the role of ω-oxidation in human fatty acid metabolism[34].

Comparative metabolomics of *hacl-1* adults. Next, we employed Metaboseek for comparative metabolomics of adult-stage *hacl-1* mutant and WT animals. Conditioned culture medium (*exo*-metabolome) and worm bodies (*endo*-metabolome) were harvested separately, extracted, and analyzed by HPLC-HRMS/MS in positive and negative ionization modes, yielding more than 500,000 features combined. Like *hacl-1* mutant larvae, *hacl-1* adults accumulate the β-branched C_{11} acid **11** and related metabolites (**Supplementary Figure 4**). However, in

contrast to L1 larvae, these C_{11} acid derivatives were not the most differential metabolites in *hacl-1* adults (**Supplementary Figure 4**).

Untargeted analysis using intensity (top 6.5% of detected features), unadjusted significance ($p < 0.05$), and fold-change (5-fold) filters uncovered >1,000 features that were enriched in the *hacl-1 exo*-metabolome, a much larger number than observed in starved L1 larvae. To parse such large numbers of differential features, Metaboseek can export annotated feature tables as inclusion lists to facilitate targeted MS/MS data acquisition. Removal of background-derived features can be accomplished using the *Peak Quality* analysis function, wherein features are scored based on fitting to an idealized peak shape. The *Peak Quality* score can be used as filtering criterion to remove features that are broad or exhibit irregular shapes. For the subsequent analysis and visualization of MS/MS data, the MS/MS networking parameters can be modified using the *Simplify Network* function, e.g., by adjusting similarity thresholds, restricting the number of edges per node, or limiting the number of nodes per cluster (**Supplementary Figure 5**).

The majority of differential features clustered in five major subnetworks (SN1-SN5, **Figure 4**). Inspection of SN1 revealed several homologous series of features, related by the mass difference of a methylene (Δ*m/z* 14.0156). Use of the "*Keep and Compare"* functionality in the *MS/MS Browser* facilitates simultaneous display of multiple MS/MS spectra and automatically highlights fragments shared between spectra, e.g., conserved daughter ions that correspond to a phosphoethanolamine moiety, a phosphorylated hexose, and ions indicating a phosphate group (**Supplementary Figure 6**). Complementary analysis of MS/MS fragmentation patterns in positive ionization mode further supported that SN1 represents *N*-acyl glycophosphoethanolamides ("*N*-acyl GPEs"), including saturated (N:0), singly unsaturated (N:1), polyunsaturated (N:n), and mono-oxygenated (mN:n) acyl moieties ranging from C_8-C_{20}. In many cases, several isobaric features were detected for each *m/z*, e.g., four distinct isomers of *N*-acyl GPE-14:2 (**Supplementary Figure 7**). Enrichment trends were similar across the *endo*- and the *exo*-metabolomes, but *N*-acyl GPE were 10-100-fold more abundant in the *exo*-metabolome (**Supplementary Figure 7**).

Finding MS/MS patterns with Metaboseek. Analysis of SN2 indicated that it represents *N*-acyl glycoglycerophosphoethanolamides ("GLEA", **Figure 4**). This compound family had been previously described in the context of ethanol-dependent *de novo* fatty acid biosynthesis in starved *C. elegans* larvae[37]. MS/MS spectra of GLEA exhibit a characteristic daughter ion at *m/z*

333.0592, in addition to phosphoglycerol and several glucose-derived fragments, which were used to define a "*Pattern*" in Metaboseek. The *Find Patterns* function in Metaboseek profiles all MS/MS spectra for user-defined fragmentation patterns, including neutral losses; hits are matched and recorded in new interactive columns in the feature table, which enabled rapid identification of more than 100 GLEA-matched molecular features distributed across SN2 and two additional subnetworks, SN3 and SN4 (**Figure 4**).

Each of the three GLEA clusters revealed slightly different MS/MS fragmentation, providing important structural clues. GLEA in SN3 produced additional daughter ions with *m/z* 376.1016 and 418.1123, suggesting β-hydroxyl substitution based on fragmentation between the α and β carbons (**Figure 4**). Larger cultures of *hacl-1* were grown and extracted to isolate the most abundant compound from SN3, GLEA-m16:1, one of the most intense and differential features in the entire *exo*-metabolome. 2D NMR spectroscopic analysis established this compound as a 2-*O*-(β-glucosyl)-glycero-1-phosphoethanolamide of β-hydroxylated hexadecenoic acid (**16**, **Supplementary Table S3**). β-hydroxylation of the fatty acyl moiety in this compound is consistent with observed fragmentation between the α and β carbons of the fatty acyl group and suggests that other metabolites in SN3 also represent GLEA of β-hydroxylated fatty acids (**Figure 4**). Upregulation of β-hydroxylated lipid derivatives suggested that mitochondrial or peroxisomal β-oxidation may be perturbed in *hacl-1* mutants. However, production of ascaroside pheromones, which relies on peroxisomal β-oxidation, was largely unchanged in *hacl-1* mutants compared to WT (**Supplementary Figure 8**), suggesting that *hacl-1* inactivation may interact with mitochondrial β-oxidation.

GLEA in SN4 did not undergo fragmentation across the α and β carbons, but instead produced an intense daughter ion with *m/z* 376.1016, corresponding to fragmentation across the amide bond. GLEA in SN4 were much less abundant and eluted later than isobaric metabolites in SN3. We hypothesize that SN4 represents GLEA bearing α-hydroxy acyl substituents; however, their low abundance precluded NMR spectroscopic characterization (**Supplementary Figure 9**). Lastly, analysis of SN5 revealed a large family of *hacl-1*-enriched *N*-acyl ethanolamides (NAEs) (**Figure 4**). All NAE in SN5 produced the daughter ion with *m/z* 102.056, corresponding to cleavage between the α- and β-carbon of the acyl group, suggesting β-hydroxylation in analogy to SN3.

Stable isotope tracing with Metaboseek. Comparing the series of *N*-acyl-GPEs, GLEA, and NAEs upregulated in *hacl-1* worms, we noted that derivatives of mono-unsaturated C_{13}- and

C_{15}-fatty acids were among the most abundant *hacl-1*-enriched compounds, even though the corresponding free fatty acids are not particularly abundant in *C. elegans*[38]. Generally, odd-chain fatty acids in *C. elegans* are derived primarily either from iso-branched chain fatty acid (BCFA) biosynthesis, which employs leucine-derived isovaleryl-CoA as a starter unit[39], or, alternatively, from metabolism of diet-derived cyclopropane fatty acids, which are abundantly produced by the bacterial diet, *E. coli* OP50[40].

We first tested whether the major *hacl-1*-enriched monounsaturated C_{13} and C_{15} lipids are derived from BCFA metabolism. For this purpose, we grew worms supplemented with $^{13}C_6$-labeled leucine, which we reasoned should result in $^{13}C_5$-enrichment of BCFAs and any derived *N*-acyl GPE, GLEA, and NAE (**Figure 5A**). The *Label Finder* tool in Metaboseek facilitated profiling $^{13}C_5$- and $^{13}C_6$-enrichment for discovery of BCFA- and Leu-derived metabolites. This analysis revealed several hundred isotope-enriched features, including iso-branched fatty acids and derivatives thereof, which were visually validated using the *Mass Shifts* feature in Metaboseek to display EICs corresponding to incorporation of $^{13}C_5$ (Δ *m/z*, 5.0167, **Figure 5B**). However, the most abundant *hacl-1*-enriched compounds harboring 13:1 and 15:1 acyl groups showed no evidence for label incorporation, indicating that these unsaturated odd chain lipids do not originate from BCFA metabolism (**Supplementary Figure 10**).

Cyclopropane fatty acids accumulate in *hacl-1.* We then asked whether the monounsaturated C_{13} and C_{15} fatty acyl derivatives accumulating in *hacl-1* mutants are derived from bacterial cyclopropane fatty acids. In the case of *E. coli* OP50, C_{17} and C_{19} cyclopropane lipids can account for nearly half of all lipid species and thus comprise a substantial portion of *C. elegans* lipid intake[41]. To test whether the monounsaturated C_{13} and C_{15} lipids upregulated in *hacl-1* are derived from cyclopropane fatty acids, we compared the metabolomes of worms fed either OP50 or JW1653-1 bacteria, a cyclopropane-deficient *E. coli* strain[42] (**Figure 5C**). First, we confirmed via 2D NMR spectroscopy that JW1653-1 does not produce cyclopropane lipids and that worms fed JW1653-1 bacteria do not produce cyclopropane lipids (**Supplementary Figure 11**). Next, we compared the metabolomes of animals grown on OP50 or JW1653-1 via HPLC-HRMS, which revealed that production of the most abundant *hacl-1*-enriched *N*-acyl GPEs was abolished in JW1653-1-fed worms (**Figure 5D**). Additional *N*-acyl GPEs enriched in *hacl-1* mutant were also found to be dependent on bacterial cyclopropane fatty acid biosynthesis, including multiple hydroxylated *N*-acyl GPE species (**Figure 5E**). Untargeted comparative analysis of OP50- and JW1653-1-fed worms revealed a large number of other cyclopropane-containing metabolites, including GLEA, as well as putative oxidized fatty acids

and fatty acyl glycosides, many of which also accumulate in *hacl-1* worms (**Figure 5F** and **Supplementary Figure 12**). Taken together, our results suggest a simple model in which diet-derived C_{17} or C_{19} cyclopropane fatty acids are initially chain shortened via β-oxidation to yield shorter chained derivatives that become substrates for pαo. If pαo is blocked, as in the case of *hacl-1* inactivation, β-oxidation intermediates are shunted towards production of, e.g., *N*-acyl GPE, GLEA, and other lipids (**Figure 5G**).

DISCUSSION

We here demonstrated the use of Metaboseek for a multi-layered comparative metabolomics study of a conserved fatty acid metabolism pathway, pαo, in *C. elegans*. By probing metabolism of WT and *hacl-1* mutants with a pαo test substrate, CA, we confirmed the predicted enzymatic function of HACL-1 as a 2-hydroxyacyl-CoA lyase. Subsequent untargeted comparison revealed pervasive changes in lipid metabolism in *hacl-1* mutants, including accumulation of an unusual family of α-hydroxylated β-branched C_{11} acids. Their abundant production and life stage-specific regulation suggests that β-branched C_{11} acids – perhaps a precursor or downstream metabolite of **11** and **12** – may serve specific functions in *C. elegans*.

In addition to the C_{11} acids, *hacl-1* mutants accumulate an unexpected diversity of modular lipids derived from the intersection of multiple branches of fatty acid metabolism with NAE biosynthesis. Particularly abundant among lipids accumulating in *hacl-1* are derivatives of cyclopropyl fatty acids, suggesting that pαo participates in cyclopropyl metabolism. Mechanisms for the breakdown of cyclopropyl fatty acids have remained largely unknown, though cyclopropyl lipids have previously been shown to profoundly affect larval development, and thus breakdown of the cyclopropyl moiety via pαo may serve a regulatory function[43]. Cyclopropyl lipids are also present in the human diet, most prominently in cheese and dairy, originating from animals fed fermented grains[44]. However, their metabolic fate in humans remains poorly understood. Cyclopropyl lipids are highly persistent in rats and accumulate as shorter-chain derivatives in adipose tissue over the course of the animal's life[45,46], and recent human studies indicate that cyclopropane lipids are more abundant in both adipose tissue and serum of obese individuals[47,48]. Our results suggest that pαo may also play a role in mammalian metabolism of cyclopropyl lipids.

Cyclopropyl and β-branched C_{11} lipids represent only some of the most abundant and most strongly *hacl-1*-dependent compounds we detected. Our comparative analysis revealed many more significant differences between the metabolomes of WT and *hacl-1*, as documented

in the Metaboseek output table (**Supplementary Table S4**). This includes retention time, *m/z*, putative molecular formulae, fold-change, as well as isotopic enrichment data, which will facilitate follow-up studies, in conjunction with the deposited MS raw data[49,50]. As we showed for the comparative analysis of *hacl-1* mutants, in-depth evaluation of MS raw data is key to feature prioritization and compound discovery. For this purpose Metaboseek combines more than 60 different modules, which tool developers can use as building blocks for specialized data analysis apps with minimal effort. Metaboseek thus provides a flexible and expandable open-source platform to accelerate annotation of the large space of yet unidentified biogenic small molecules.

Our comparative metabolomic analysis of α-oxidation shows that even a primary metabolic pathway in an otherwise well-studied model system can reveal a large number of previously uncharacterized compounds, as well as unexpected connections to other pathways, e.g., β-oxidation or cyclopropane fatty acid metabolism. Like much of conserved primary metabolism, α-oxidation was initially characterized more than 50 years ago[51,52]. It seems likely that re-analysis of primary metabolic pathways using state-of-the-art MS and data analysis tools can significantly advance our understanding of biochemical networks and help harness the potential of metabolomics as the ‘omics discipline that most closely reflects phenotype[7–9].

METHODS

***C. elegans* strains.** Unless otherwise indicated, worms were maintained on Nematode Growth Medium (NGM) 6 cm diameter petri dish plates seeded with *E. coli* OP50 obtained from the *Caenorhabditis* Genetics Center (CGC). For experiments with cyclopropane deficient bacteria, worms were grown on NGM 6cm plates seeded with *E. coli* JW1653-1, a kind gift from the Walhout Lab (University of Massachusetts Medical School, Worcester, MA). The following *C. elegans* strains were used for comparative metabolomics: Bristol N2 ("wildtype") obtained from the CGC, and *B0334.3(tm6725)*, referred to as *hacl-1,* strain designation FRA7. The FRA7 strain was the result of backcrossing *hacl-1* with *sqt-1 (*FRA6) for seven generations. FRA6 was iteratively backcrossed with Bristol N2 for a total of six generations. After the final backcross, FRA7 hermaphrodites were singled and allowed to self, non-rollers were picked, and the genotype was confirmed by PCR and Sanger sequencing.

***C. elegans* liquid cultures.** Analysis of starved L1 larvae followed a previously described procedure[53]. For the analysis of staged gravid adults, approximately 75,000 synchronized L1 larvae were added to 125 mL Erlenmeyer flasks containing 25 mL S-complete medium and kanamycin at 35 µg/mL to prevent contamination. Worms were fed with 50x concentrated *E. coli* OP50 or *E. coli* JW1653-1 and incubated at 20 °C with shaking at 180 RPM for 66–70 h, at which time the population was predominantly gravid adults, determined by microscopic inspection. Control samples to account for bacterial matrix were prepared with the same amount of *E. coli* OP50 or JW1653-1 under identical conditions. Liquid cultures were transferred to 50 mL conical tubes and centrifuged (500 x g, 22 °C, 1 min), and the top 20 mL of the resulting supernatant (*exo*-metabolome) was transferred to a fresh conical tube and snap frozen. Remaining worm pellet was transferred to a 15 mL conical tube, centrifuged (500 x g, 22 °C, 1 minute), and washed three times with M9 before snap freezing in liquid nitrogen.

Test substrate feeding experiments. Approximately 100,000 synchronized L1 larvae were added to 125 mL Erlenmeyer flasks containing 10 mL M9 media and 300 µM citronellic acid (Sigma-Aldrich 303429), phytanic acid (Sigma-Aldrich P4060), retinoic acid (Sigma-Aldrich R2625), geranic acid (Aldrich 427764), or an equivalent volume of methanol only (vehicle control) and were incubated at 20 °C with shaking at 180 RPM for 24 hrs. Cultures were transferred to 15 mL conical tubes and centrifuged (500 x g, 22 °C, 1 min), and the resulting supernatant (*exo*-metabolome) was transferred to a fresh conical tube and snap frozen. Remaining L1 pellet was washed three times with M9 before snap freezing in liquid nitrogen.

$^{13}C_6$-Leu isotope tracing experiment. Approximately 60,000 synchronized N2 (WT) L1 larvae were added to 125 mL Erlenmeyer flasks containing 20 mL S-Complete medium. Worms were fed with 60 mg freeze-dried OP50 powder (InVivoBiosystems, formerly NemaMetrix Inc., OP-50-31772) and supplemented with leucine (Sigma Aldrich L8000) or $^{13}C_6$-leucine (Cambridge Isotope Laboratories CLM-2262-H-PK) at a final concentration of 2 mM. Worms were incubated at 20 °C with shaking at 180 RPM for 66–70 hrs, at which time the population was a mixture of young and gravid adults, determined by microscopic inspection. Liquid cultures were centrifuged (500 x g, 22 °C, 1 min), and the resulting supernatant was snap frozen. Worm pellet was washed three times with M9 before snap freezing in liquid nitrogen.

Sample preparation for HPLC-MS. *Exo*-metabolome (conditioned media) samples were lyophilized ~48 hrs using a VirTis BenchTop 4K Freeze Dryer. Dried material was directly extracted in 10 mL methanol in 20 mL glass vials stirred overnight. Vials were centrifuged at 2750 RCF for five minutes in an Eppendorf 5702 Centrifuge using rotor F-35-30-17. The resulting supernatant was transferred to a clean 20 mL glass vial and concentrated to dryness in an SC250EXP Speedvac Concentrator coupled to an RVT5105 Refrigerated Vapor Trap (Thermo Scientific). The resulting powder was suspended in methanol and analyzed directly by HPLC-MS, as described below. *Endo*-metabolome (nematode bodies) were lyophilized for 18-24 hrs using a VirTis BenchTop 4K Freeze Dryer. Dried pellets were transferred to 1.5 mL microfuge tubes and disrupted in a Spex 1600 MiniG tissue grinder after the addition of two stainless steel grinding balls to each sample. Microfuge tubes were placed in a Cryoblock (Model 1660) cooled in liquid nitrogen, and samples were disrupted at 1100 RPM for 60 s. This process was repeated two additional rounds for a total of three disruptions. Pellets were transferred to 8 mL glass vials in 5 mL methanol and stirred overnight. Subsequent steps for concentration and resuspension were followed as described for the *exo*-metablome.

Mass spectrometry. Liquid chromatography was performed on a Vanquish HPLC system controlled by Chromeleon Software (ThermoFisher Scientific) and coupled to an Orbitrap Q-Exactive High Field mass spectrometer controlled by Xcalibur software (ThermoFisher Scientific). Methanolic extracts prepared as described above were separated on a Thermo Hypersil Gold C18 column (150 mm x 2.1 mm, particle size 1.9 µM; 25002-152130) maintained at 40 °C with a flow rate of 0.5 mL/min. Solvent A: 0.1% formic acid (Fisher Chemical Optima LC/MS grade; A11750) in water (Fisher Chemical Optima LC/MS grade; W6-4); solvent B: 0.1% formic acid in acetonitrile (Fisher Chemical Optima LC/MS grade; A955-4). A/B gradient started at 1% B for 3 min after injection and increased linearly to 98% B at 20 min, followed by 5 min at

98% B, then back to 1% B over .1 min and finally held at 1% B for the remaining 2.9 min to re-equilibrate the column (28 min total method time). Mass spectrometer parameters: spray voltage, -3.0 kV / +3.5 kV; capillary temperature 380 °C; probe heater temperature 400 °C; sheath, auxiliary, and sweep gas, 60, 20, and 2 AU, respectively; S-Lens RF level, 50; resolution, 120,000 at *m/z* 200; AGC target, 3E6. Each sample was analyzed in negative (ESI-) and positive (ESI+) electrospray ionization modes with *m/z* range 100-1000. Parameters for MS/MS (dd-MS2): MS1 resolution, 60,000; AGC Target, 1E6. MS2 resolution, 30,000; AGC Target, 2E5. Maximum injection time, 60 msec; Isolation window, 1.0 *m/z*; stepped normalized collision energy (NCE) 10, 30; dynamic exclusion, 5 sec; top 8 masses selected for MS/MS per scan. Inclusion lists with 20 sec windows were generated in Metaboseek for targeted MS/MS.

Metaboseek analysis. HPLC-MS data were analyzed using Metaboseek software (documentation available at Metaboseek.com) after conversion to mzXML file format using MSConvert (version 3.0, ProteoWizard[54]); for a full list of supported file types, see section 3.3.4 *Supported File Types*. A subset of the mzXML files used in this study are provided as an example data set included with the Metaboseek download at Metaboseek.com. Following conversion to mzXML, data were analyzed using the xcms-module within Metaboseek with default settings, as described in section 3.5 *XCMS Analysis*. The xcms-generated feature table was loaded into the Metaboseek *Data Explorer* along with relevant MS files by designating a project folder, see section 3.3.2 *Load a Metaboseek Project Folder*. MS data display and MS data table were grouped according to genotype and experimental condition via *Regroup MS data* (section 3.4.2) and *Regroup Table* (section 3.4.4.4), respectively. Basic analysis was performed after designating WT as the “control” group; see section 3.4.4.3 *Analyze Table* for a complete list of analysis and normalization options. Following basic analysis, relevant MS/MS data were loaded as described in section 3.3.1 *Load MS Data Files Directly*, followed by matching of MS/MS scans to the MS1 files as described in section 3.4.4.3.3 *Advanced Analysis* under the subheading *Find MS2 scans*. At this point, the table was culled to include only MS/MS-matched features, then culled further using the *Fast Peak Shapes* (Peak Quality) analysis and a retention time filter, as described in section 3.4.4 *Feature Table Actions*. MS/MS networking was performed as described in section 3.4.2.2 *Compare MS2,* see also **Supplementary Figure 5** for an example of the *Simplify Network* modifications and display options. All plots and reports, including SIRIUS fragmentation trees, can be exported as vector graphics for rapid and efficient sharing, outlined in section 3.4.2.2 *Feature Report*.

Isolation and NMR spectroscopy of bemeth#3 (11) and GLEA-m16:1 (16). For isolation of GLEA-m16:1 (**16**) from adult *exo*-metabolome, conditioned media from several medium scale *C. elegans hacl-1* cultures was lyophilized and extracted with methanol (as described). Dried methanol extract was loaded onto Celite and fractionated using medium pressure reverse phase chromatography (15 g C18 Combiflash RediSep column, Teledyne Isco 69-2203-334). Solvent A: 0.1% acetic acid in water; solvent B: acetonitrile. Column was primed with 1% B; separation was achieved by 5% B for 2 column volumes (CV), which was increased linearly to 50% B over 15 CV, then to 100% B over 3 CV and held at 100% B for 5 CV, before returning to 80% B for 3 CV. Fractions were assayed for compounds of interest by HPLC-MS, the relevant fractions were combined and dried *in vacuo*. Following suspension in water: methanol (1:2), the pooled fractions were further separated by semi-preparative HPLC on a Thermo Hypersil Gold C18 column (250 mm x 10 mm, particle size 5 µM; 25005-259070) using a Vanquish UPLC system controlled by Chromeleon Software (ThermoFisher Scientific) and coupled to a Dionex UltiMate 3000 Automated fraction collector and to an Orbitrap Q-Exactive High Field mass spectrometer using a 9:1 split. Fractions containing GLEA-m16:1 were combined and analyzed by 2D NMR spectroscopy (CD_3OD, Bruker AVANCE III HD, 800 MHz). For spectroscopic data, see **Supplementary Table S3**. For isolation of bemeth#3, conditioned media from several starved L1 cultures was extracted and fractionated analogously. For spectroscopic data, see **Supplementary Table S1**, and relevant section of the dqfCOSY spectrum are shown in **Supplementary Figure S2**.

Chemical syntheses

General synthetic procedures. All oxygen and moisture-sensitive reactions were carried out under argon atmosphere in flame-dried glassware. Solutions and solvents sensitive to moisture and oxygen were transferred via standard syringe and cannula techniques. All commercial reagents were purchased as reagent grade and, unless otherwise stated, were purchased from Sigma-Aldrich and used without any further purification. Acetic acid (AcOH), acetonitrile (ACN), dichloromethane (DCM), ethyl acetate (EtOAc), formic acid, hexanes and methanol (MeOH) used for chromatography and as a reagent or solvent were purchased from Fisher Scientific. Thin-layer chromatography (TLC) was performed using J. T. Baker Silica Gel IB2F plates. Flash chromatography was performed using Teledyne Isco CombiFlash systems and Teledyne Isco RediSep Rf silica and C18 columns. All deuterated solvents were purchased from Cambridge Isotopes. Nuclear Magnetic Resonance (NMR) spectra were recorded on Bruker INOVA 500 (500 MHz) and Varian INOVA 600 (600 MHz) spectrometers at Cornell University's NMR facility and Bruker AVANCE III HD 800 MHz (800 MHz) or Bruker AVANCE III HD 600 MHz (600 MHz) at SUNY ESF's NMR facility. ^{1}H NMR chemical shifts are reported in ppm (δ) relative to residual solvent peaks (7.26 ppm for chloroform-d, 3.31 ppm for methanol-d_4). NMR-spectroscopic data are reported as follows: chemical shift, multiplicity (s = singlet, d = doublet, t = triplet, q = quartet, m = multiplet, br = broad), coupling constants (Hz). ^{13}C NMR chemical shifts are reported in ppm (δ) relative to residual solvent peaks (77.16 ppm for chloroform-d, 49.00 ppm for methanol-d_4). All NMR data processing was done using MNOVA 14.2.1 (https://mestrelab.com/).

Preparation of [Cu(*S,S*)-*tert*-butylbis(oxazolinyl)](SbF$_6$)$_2$

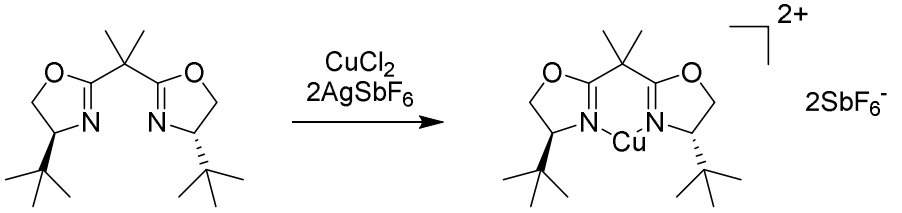

[Cu(S,S)-tert-butylbis(oxazolinyl)](SbF $_6$)$_2$

To a solution of (*S,S*)-2,2′-isopropylidene-bis(4-tert-butyl-2-oxazoline) (200 mg, 0.68 mmol) in dry dichloromethane (8 mL), $CuCl_2 \cdot H_2O$ (139 mg, 0.82 mmol) and $AgSbF_6$ (583 mg, 0.7 mmol)

were added, and the resulting mixture was stirred at room temperature for 14 hours. The green solution was filtered through cotton for later use.

Ethyl 2-hydroxy-3-methylpent-4-enoate (14)

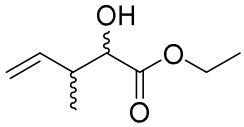

cis-butene was bubbled through a solution of ethyl glyoxylate (2 mL, 9.82 mmol) and [Cu(*S,S*)-*tert*-butylbis(oxazolinyl)]$(SbF_6)_2$ at -78 °C in dry dichloromethane (2 mL), and the reaction was sealed to react at 40 °C. After 2 days, the reaction was concentrated *in vacuo*. Flash column chromatography on silica using a gradient of 0-30% ethyl acetate in hexane afforded **14** as a clear oil (977 mg, 63%, mixture of diastereomers).

Major diastereomer, ^{1}H NMR (600 MHz, chloroform-*d*): δ (ppm) 5.74 (ddd, *J* = 17.8, 9.8, 8.1 Hz, 1H), 5.07 (m, 1H), 5.05 (m, 1H), 4.24 (m, 2H), 4.10 (dd, *J* = 6.2, 3.4 Hz, 1H), 2.72 (d, *J* = 6.2 Hz, 1H), 2.69-2.61 (m, 1H), 1.29 (t, *J* = 7.2 Hz, 3H), 1.16 (d, *J* = 7.0 Hz, 3H).

Minor diastereomer, ^{1}H NMR (600 MHz, chloroform-*d*): δ (ppm) 5.85 (ddd, *J* = 17.4, 10.3, 7.4 Hz, 1H), 5.12 (m, 1H), 5.09 (m, 1H), 4.26 (m, 2H), 4.16 (dd, *J* = 6.3, 3.7 Hz, 1H), 2.76 (d, *J* = 6.3 Hz, 1H), 2.69-2.61 (m, 1H), 1.29 (t, *J* = 7.2 Hz, 3H), 1.01 (d, *J* = 7.0 Hz, 3H).

Ethyl (*E*)-2-hydroxy-3-methyldec-4-enoate (15)

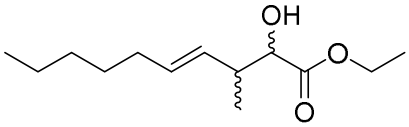

To a solution of **14** (950 mg, 6.00 mmol) dissolved in dry dichloromethane (20 mL), Grubbs catalyst 2nd generation (94 mg, 0.15 mmol) and 1-heptene (2.52 mL, 18.00 mmol) were added at room temperature. The reaction mixture was allowed to stir 20 h and was concentrated *in vacuo*. Flash column chromatography on silica using a gradient of 0-30 % ethyl acetate in hexanes afforded **15** as a clear oil (785 mg, 76% BRSM, mixture of diastereomers).

Major diastereomer, ^{1}H NMR (600 MHz, chloroform-*d*): δ (ppm) 5.46 (dt, *J* = 15.4, 6.7 Hz, 1H), 5.31 (dd, *J* = 15.4, 8.2 Hz, 1H), 4.27-4.18 (m, 2H), 4.06 (m, 1H), 2.67 (d, *J* = 5.2 Hz, 1H), 2.60

(m, 1H), 1.96 (q, *J* = 7.3 Hz, 2H), 1.36-1.20 (m, 6H), 1.29 (t, *J* = 7.3 Hz, 3H), 1.13 (d, *J* = 7.1 Hz, 3H), 0.87 (t, *J* = 7.2 Hz, 3H).

Minor diastereomer, ^{1}H NMR (600 MHz, chloroform-*d*): δ (ppm) 5.52 (dt, *J* = 15.4, 6.5 Hz, 1H), 5.40 (dd, *J* = 15.4, 7.8 Hz, 1H), 4.27-4.18 (m, 2H), 4.09 (m, 1H), 2.70 (d, *J* = 6.8 Hz, 1H), 2.56 (m, 1H), 2.00 (q, *J* = 7.2 Hz, 2H), 1.36-1.20 (m, 6H), 1.28 (t, *J* = 7.2 Hz, 3H), 1.12 (d, *J* = 7.0 Hz, 3H), 0.87 (t, *J* = 7.1 Hz, 3H).

(*E*)-2-hydroxy-3-methyldec-4-enoic acid (bemeth#2, 12)

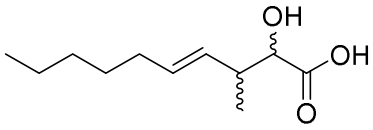

To a solution of **15** (76 mg, 0.33 mmol) in 1,4-dioxane (2 mL), lithium hydroxide monohydrate (42 mg, 1.00 mmol) in H_2O (1 mL) was added, and the resulting mixture was stirred at 60 °C for 12 hours. Glacial acetic acid (0.5 mL) was added, and the reaction was concentrated *in vacuo*. Flash column chromatography on silica using a gradient of 0-50% ethyl acetate in hexanes afforded **12** (46.7 mg, 70%) as a clear oil.

For ^{1}H and ^{13}C NMR spectroscopic data of the major diastereomer of bemeth#2 (**12)**, see **Supplementary Table S2**.

Minor diastereomer, ^{1}H NMR (600 MHz, methanol-d_4): δ (ppm) δ (ppm) 5.56-5.41 (m, 2H), 3.96 (d, *J* = 4.6 Hz, 1H), 2.54 (m, 1H), 2.00 (m, 2H), 1.43-1.25 (m, 6H), 1.00 (d, *J* = 6.9 Hz, 3H), 0.90 (t, *J* = 7.0 Hz, 3H).

Data availability. All data analyzed during this study are included in the manuscript and supporting files. MS/MS data is available via MassIVE under accession number: MSV000087885. Helf MJ, Fox BW, Artyukhin AB, Zhang YK, Schroeder FC (2021) MassIVE ID MSV000087885. Comparative metabolomics with Metaboseek reveals functions of peroxisomal α-oxidation in *C. elegans*.

Code availability. Metaboseek is available as an R package, as an installer and bundled into a .zip file for Windows. All source code and downloads are available at https://github.com/mjhelf/Metaboseek. Code documentation and a tutorial vignette are part of the Metaboseek R package. The tutorial is also available at https://metaboseek.com/doc.

Acknowledgements. This research was supported in part by the National Institutes of Health (R35GM131877 and U01GM110714 to F.C.S.). F.C.S. is a Faculty Scholar of the Howard Hughes Medical Institute. M.J.H received a Research Fellowship from the Deutsche Forschungsgemeinschaft (DFG), Project Number 386228702. Some strains used in this work were provided by the CGC, which is funded by the NIH Office of Research Infrastructure Programs (P40 OD010440). *B0334.3(tm6725)* was obtained from the National Bioresource Project, Tokyo, Japan. We thank Diana Carolina Fajardo Palomino and Gary Horvath for technical support and David Kiemle for assistance with NMR spectroscopy. We thank Dr. Yong-Uk Lee and the Walhout lab for kindly sharing the JW1653-1 *E. coli* strain.

Author Contributions. FCS supervised the study. MJH and FCS conceived the Metaboseek platform. MJH developed the Metaboseek platform. BWF and ABA performed chemical and biological experiments. YKZ performed syntheses. BWF, MJH, and FCS wrote the paper with input from all authors.

Competing Interests. The authors declare no competing interests.

References

1. Zamboni, N., Saghatelian, A. & Patti, G. J. Defining the Metabolome: Size, Flux, and Regulation. *Molecular Cell* vol. 58 699–706 (2015).

2. Joshua, W. *et al.* A novel 3-hydroxysteroid dehydrogenase that regulates reproductive development and longevity. *PLoS Biol.* (2012).

3. Watson, E. *et al.* Interspecies systems biology uncovers metabolites affecting C. elegans gene expression and life history traits. *Cell* (2014) doi:10.1016/j.cell.2014.01.047.

4. O'Donnell, M. P., Fox, B. W., Chao, P. H., Schroeder, F. C. & Sengupta, P. A neurotransmitter produced by gut bacteria modulates host sensory behaviour. *Nature* (2020) doi:10.1038/s41586-020-2395-5.

5. Funabashi, M. *et al.* A metabolic pathway for bile acid dehydroxylation by the gut microbiome. *Nature* **582**, 566–570 (2020).

6. Patti, G. J., Yanes, O. & Siuzdak, G. Innovation: Metabolomics: the apogee of the omics trilogy. *Nature Reviews Molecular Cell Biology* (2012) doi:10.1038/nrm3314.

7. Guijas, C., Montenegro-Burke, J. R., Warth, B., Spilker, M. E. & Siuzdak, G. Metabolomics activity screening for identifying metabolites that modulate phenotype. *Nat. Biotechnol. 2018 364* **36**, 316–320 (2018).

8. Wishart, D. S. Metabolomics for investigating physiological and pathophysiological processes. *Physiol. Rev.* **99**, 1819–1875 (2019).

9. Johnson, C. H., Ivanisevic, J. & Siuzdak, G. Metabolomics: Beyond biomarkers and towards mechanisms. *Nature Reviews Molecular Cell Biology* (2016) doi:10.1038/nrm.2016.25.

10. Harayama, T. & Riezman, H. Understanding the diversity of membrane lipid composition. *Nature Reviews Molecular Cell Biology* vol. 19 281–296 (2018).

11. Walker, D. I. *et al.* The metabolome: A key measure for exposome research in epidemiology. *Curr. Epidemiol. reports* **6**, 93 (2019).

12. Baker, M. Metabolomics: From small molecules to big ideas. *Nat. Methods* (2011) doi:10.1038/nmeth0211-117.

13. Smith, C. a, Want, E. J., O'Maille, G., Abagyan, R. & Siuzdak, G. XCMS: processing mass spectrometry data for metabolite profiling using nonlinear peak alignment, matching, and identification. *Anal. Chem.* **78**, 779–87 (2006).

14. Tautenhahn, R., Bottcher, C. & Neumann, S. Highly sensitive feature detection for high resolution LC/MS. *BMC Bioinformatics* **9**, 504 (2008).

15. Pluskal, T., Castillo, S., Villar-Briones, A. & Orešič, M. MZmine 2: Modular framework for processing, visualizing, and analyzing mass spectrometry-based molecular profile data. *BMC Bioinformatics* **11**, (2010).

16. Tsugawa, H. *et al.* MS-DIAL: Data-independent MS/MS deconvolution for comprehensive metabolome analysis. *Nat. Methods* **12**, 523–526 (2015).

17. Tsugawa, H. *et al.* A lipidome atlas in MS-DIAL 4. *Nat. Biotechnol. 2020 3810* **38**, 1159–1163 (2020).

18. Chong, J. *et al.* MetaboAnalyst 4.0: Towards more transparent and integrative metabolomics analysis. *Nucleic Acids Res.* **46**, W486–W494 (2018).

19. Tautenhahn, R., Patti, G. J., Rinehart, D. & Siuzdak, G. XCMS online: A web-based platform to process untargeted metabolomic data. *Anal. Chem.* **84**, 5035–5039 (2012).

20. Tsugawa, H. *et al.* Hydrogen Rearrangement Rules: Computational MS/MS Fragmentation and Structure Elucidation Using MS-FINDER Software. *Anal. Chem.* **88**, 7946–7958 (2016).

21. Djoumbou-Feunang, Y. *et al.* Cfm-id 3.0: Significantly improved esi-ms/ms prediction and compound identification. *Metabolites* **9**, (2019).

22. Dührkop, K. *et al.* SIRIUS 4: a rapid tool for turning tandem mass spectra into metabolite structure information. *Nat. Methods* (2019) doi:10.1038/s41592-019-0344-8.

23. Wang, M. *et al.* Sharing and community curation of mass spectrometry data with Global Natural Products Social Molecular Networking. *Nature Biotechnology* vol. 34 828–837 (2016).

24. Petras, D. *et al.* GNPS Dashboard: Collaborative Analysis of Mass Spectrometry Data in the Web Browser. *bioRxiv* 2021.04.05.438475 (2021) doi:10.1101/2021.04.05.438475.

25. Kuhl, C., Tautenhahn, R., Böttcher, C., Larson, T. R. & Neumann, S. CAMERA: An Integrated Strategy for Compound Spectra Extraction and Annotation of Liquid Chromatography/Mass Spectrometry Data Sets. *Anal. Chem.* **84**, 283–289 (2012).

26. Wanders, R. J. A., Waterham, H. R. & Ferdinandusse, S. Metabolic interplay between peroxisomes and other subcellular organelles including mitochondria and the endoplasmic reticulum. *Frontiers in Cell and Developmental Biology* (2016) doi:10.3389/fcell.2015.00083.

27. Artyukhin, A. B. *et al.* Metabolomic 'dark Matter' Dependent on Peroxisomal β-Oxidation in Caenorhabditis elegans. *J. Am. Chem. Soc.* (2018) doi:10.1021/jacs.7b11811.

28. McGrath, P. T. & Ruvinsky, I. A primer on pheromone signaling in Caenorhabditis elegans for systems biologists. *Current Opinion in Systems Biology* vol. 13 23–30 (2019).

29. Foulon, V. *et al.* Purification, molecular cloning, and expression of 2-hydroxyphytanoyl-CoA lyase, a peroxisomal thiamine pyrophosphate-dependent enzyme that catalyzes the carbon-carbon bond cleavage during alpha -oxidation of 3-methyl-branched fatty acids. *Proc. Natl. Acad. Sci.* **96**, 10039–10044 (1999).

30. Mukherji, M. *et al.* The chemical biology of branched-chain lipid metabolism. *Progress in Lipid Research* (2003) doi:10.1016/S0163-7827(03)00016-X.

31. Croes, K., Foulon, V., Casteels, M., Van Veldhoven, P. P. & Mannaerts, G. P. Phytanoyl-CoA hydroxylase: Recognition of 3-methyl-branched acyl-CoAs and requirement for GTP or ATP and Mg2+ in addition to its known hydroxylation cofactors. *J. Lipid Res.* **41**, 629–636 (2000).

32. Wanders, R. J. A., Komen, J. & Ferdinandusse, S. Phytanic acid metabolism in health and disease. *Biochimica et Biophysica Acta - Molecular and Cell Biology of Lipids* (2011) doi:10.1016/j.bbalip.2011.06.006.

33. Bandu, M. L., Grubbs, T., Kater, M. & Desaire, H. Collision induced dissociation of alpha hydroxy acids: Evidence of an ion-neutral complex intermediate. *Int. J. Mass Spectrom.* (2006) doi:10.1016/j.ijms.2006.01.004.

34. Wanders, R. J. A., Komen, J. & Kemp, S. Fatty acid omega-oxidation as a rescue pathway for fatty acid oxidation disorders in humans. *FEBS Journal* (2011)

649 doi:10.1111/j.1742-4658.2010.07947.x.

650 35. Nothias, L. F. *et al.* Feature-based molecular networking in the GNPS analysis
651 environment. *Nat. Methods* **17**, 905–908 (2020).

652 36. Gao, A. W. *et al.* A sensitive mass spectrometry platform identifies metabolic changes of
653 life history traits in C. elegans. *Sci. Rep.* **7**, 1–14 (2017).

654 37. Artyukhin, A. B., Yim, J. J., Cheong Cheong, M. & Avery, L. Starvation-induced collective
655 behavior in C. elegans. *Sci. Rep.* (2015) doi:10.1038/srep10647.

656 38. Watts, J. L. & Ristow, M. Lipid and carbohydrate metabolism in Caenorhabditis elegans.
657 *Genetics* **207**, 413–446 (2017).

658 39. Kniazeva, M., Crawford, Q. T., Seiber, M., Wang, C. Y. & Han, M. Monomethyl branched-
659 chain fatty acids play an essential role in Caenorhabditis elegans development. *PLoS*
660 *Biol.* **2**, (2004).

661 40. Grogan, D. W. & Cronan, J. E. Cyclopropane ring formation in membrane lipids of
662 bacteria. *Microbiol. Mol. Biol. Rev.* **61**, 429–441 (1997).

663 41. Brooks, K. K., Liang, B. & Watts, J. L. The influence of bacterial diet on fat storage in C.
664 elegans. *PLoS One* (2009) doi:10.1371/journal.pone.0007545.

665 42. Baba, T. *et al.* Construction of Escherichia coli K-12 in-frame, single-gene knockout
666 mutants: The Keio collection. *Mol. Syst. Biol.* (2006) doi:10.1038/msb4100050.

667 43. Kaul, T. K., Reis Rodrigues, P., Ogungbe, I. V., Kapahi, P. & Gill, M. S. Bacterial fatty
668 acids enhance recovery from the dauer larva in Caenorhabditis elegans. *PLoS One*
669 (2014) doi:10.1371/journal.pone.0086979.

670 44. Caligiani, A., Nocetti, M., Lolli, V., Marseglia, A. & Palla, G. Development of a
671 Quantitative GC-MS Method for the Detection of Cyclopropane Fatty Acids in Cheese as
672 New Molecular Markers for Parmigiano Reggiano Authentication. *J. Agric. Food Chem.*
673 (2016) doi:10.1021/acs.jafc.6b00913.

674 45. Wood, R. & Reiser, R. Cyclopropane fatty acid metabolism: Physical and chemical
675 identification of propane ring metabolic products in the adipose tissue. *J. Am. Oil Chem.*
676 *Soc.* (1965) doi:10.1007/BF02540137.

677 46. Chung, A. E. Metabolism of cyclopropane fatty acids oxidation of cis-9,10-methylene
678 hexadecanoic and cis-9,10-methylene octadecanoic acids by rat-liver mitochondria.
679 *Biochim. Biophys. Acta (BBA)/Lipids Lipid Metab.* (1966) doi:10.1016/0005-
680 2760(66)90003-8.

681 47. Sledzinski, T. *et al.* Identification of cyclopropaneoctanoic acid 2-hexyl in human adipose
682 tissue and serum. *Lipids* **48**, 839–848 (2013).

683 48. Mika, A. *et al.* Increased Serum Level of Cyclopropaneoctanoic Acid 2-Hexyl in Patients
684 with Hypertriglyceridemia-Related Disorders. *Lipids* **51**, 867–873 (2016).

685 49. Sud, M. *et al.* Metabolomics Workbench: An international repository for metabolomics
686 data and metadata, metabolite standards, protocols, tutorials and training, and analysis
687 tools. *Nucleic Acids Res.* **44**, D463–D470 (2016).

688 50. Aron, A. T. *et al.* Reproducible molecular networking of untargeted mass spectrometry
689 data using GNPS. *Nat. Protoc.* **15**, 1954–1991 (2020).

690 51. Mize, C. E., Steinberg, D., Avigan, J. & Fales, H. M. A pathway for oxidative degradation
691 of phytanic acid in mammals. *Biochem. Biophys. Res. Commun.* **25**, 359–365 (1966).

692 52. Mize, C. E. *et al.* A major pathway for the mammalian oxidative degradation of phytanic
693 acid. *Biochim. Biophys. Acta - Lipids Lipid Metab.* **176**, 720–739 (1969).

694 53. Artyukhin, A. B., Schroeder, F. C. & Avery, L. Density dependence in Caenorhabditis
695 larval starvation. *Sci. Rep.* (2013) doi:10.1038/srep02777.

696 54. MC, C. *et al.* A cross-platform toolkit for mass spectrometry and proteomics. *Nat.*
697 *Biotechnol.* **30**, 918–920 (2012).

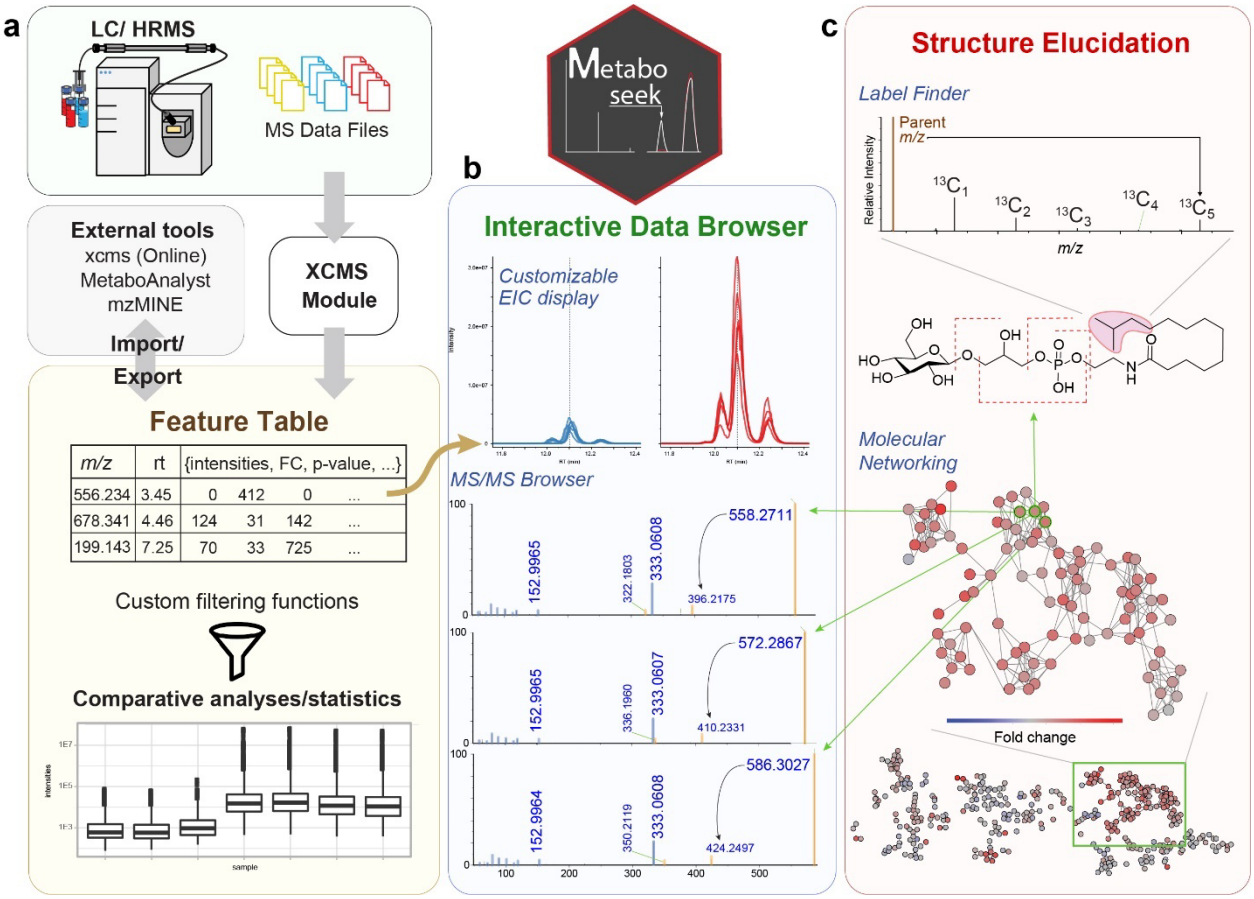

Figure 1. Comparative Metabolomics with Metaboseek. **a,** Metaboseek includes an integrated xcms module for feature detection and feature grouping (with CAMERA annotation) and accepts feature tables generated by other software. **b,** Features can be annotated and prioritized using extensive filtering options and integrated statistics tools. Raw data for each molecular feature can be browsed rapidly, including associated EICs, MS1 and MS/MS spectra. **c**, The data browser interacts with a suite of structure elucidation tools, e.g., SIRIUS-based molecular formula and structure prediction, the *Label Finder* to identify isotope-labeled compounds, and the MS/MS pattern finder to identify MS features with characteristic fragmentation patterns.

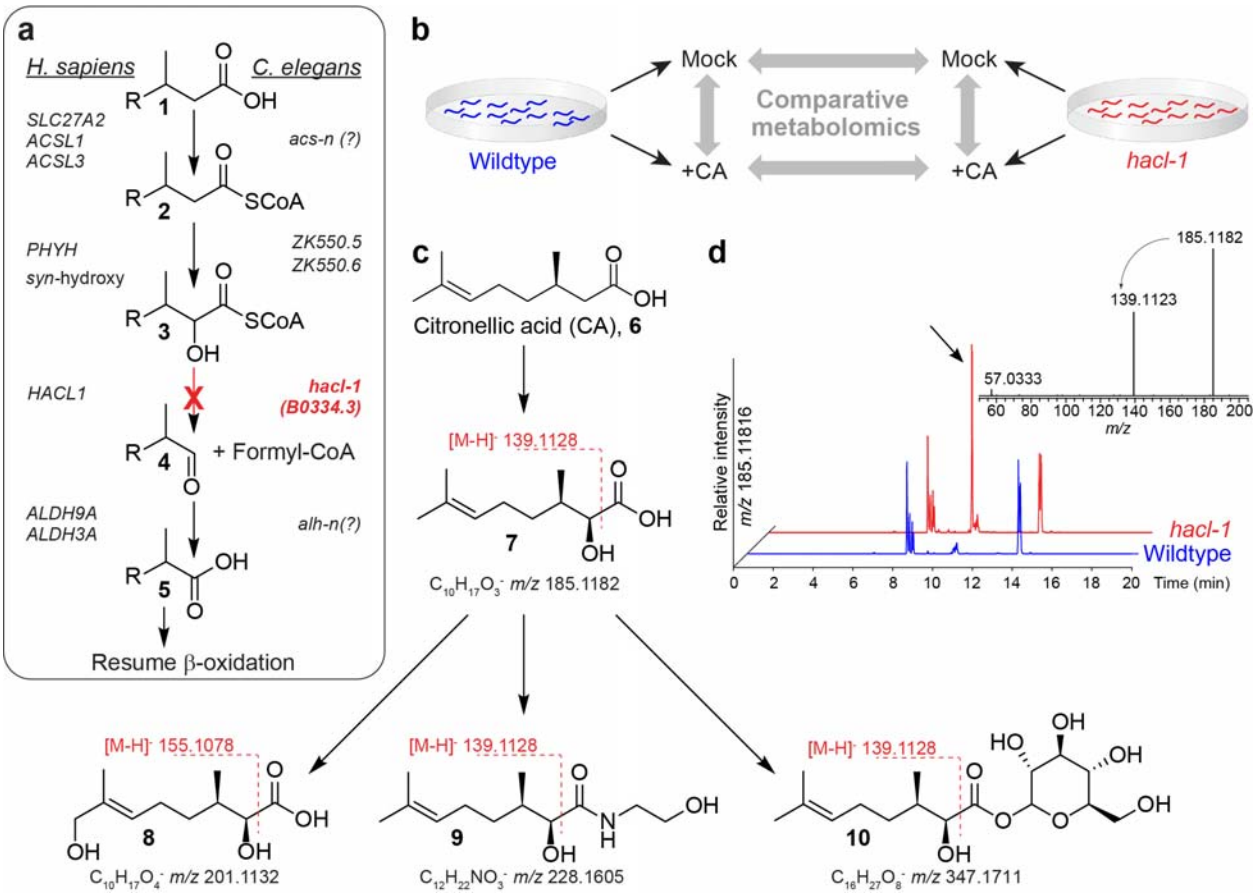

Figure 2. Comparative metabolomics of CA-fed *hacl-1* mutants. **a,** Conservation of peroxisomal α-oxidation in *C. elegans* and humans. **b,** CA-feeding experiment. *C. elegans* larvae were supplemented with CA, (**6**) followed by comparative analysis with Metaboseek. **c,** Representative shunt metabolites accumulating in *hacl-1* following CA supplementation. The majority of shunt metabolites fragment between the carbonyl- and α-carbon during MS/MS, which is characteristic of α-hydroxy fatty acids. **d,** HPLC-MS (negative ion) EIC for *hacl-1*-enriched feature with *m/z* 185.1182, corresponding to **7** (arrow). Its MS/MS spectrum reveals a daughter ion at *m/z* 139.1123, corresponding to neutral loss of formic acid.

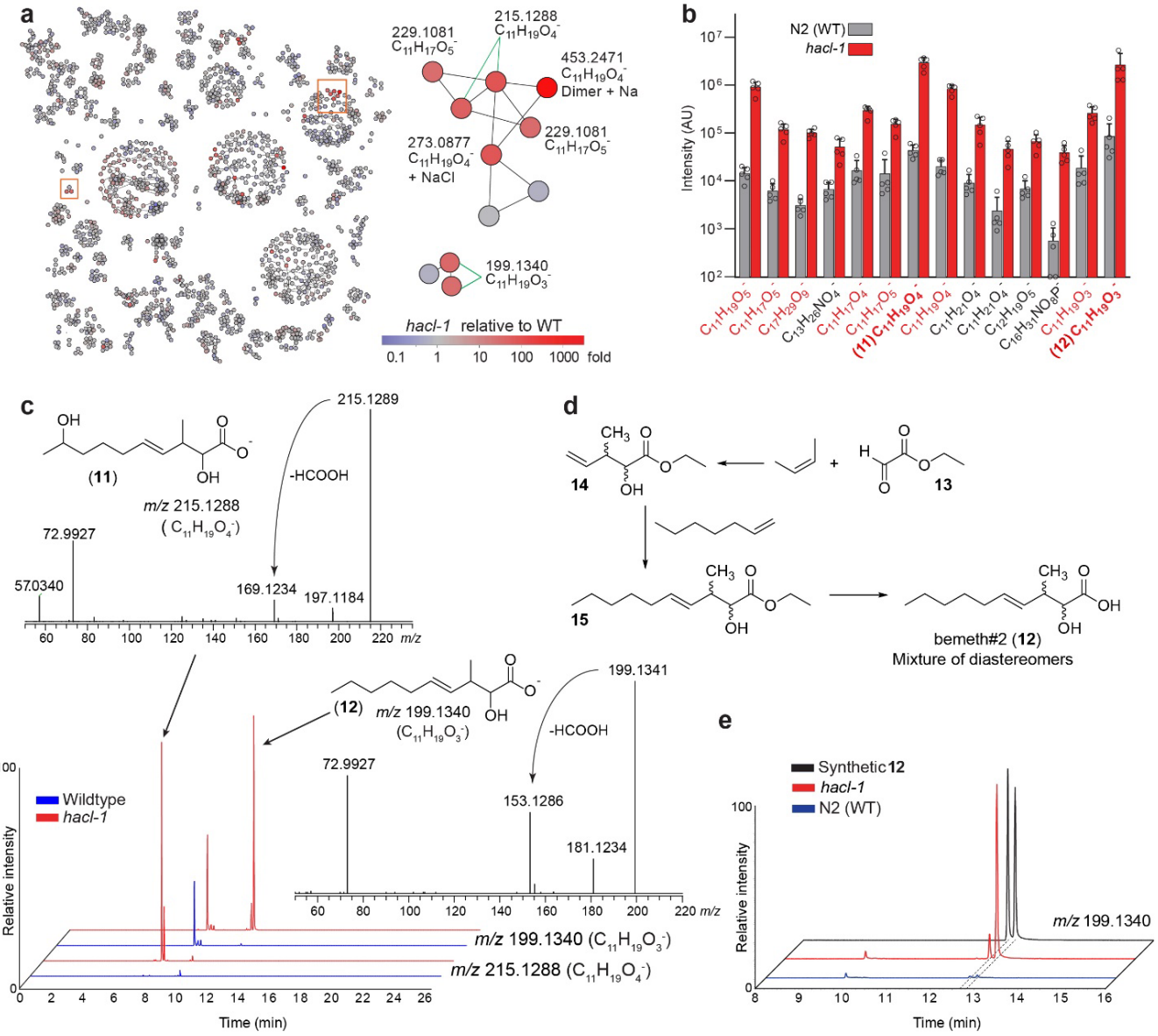

Figure 3. Endogenous metabolites accumulating in *hacl-1* mutant larvae. **a,** MS/MS network highlighting differential abundance in *hacl-1* mutants relative to WT. Subnetworks of interest (orange boxes) are shown enlarged. **b,** Quantification of endogenous metabolites ten-fold or more enriched in *hacl-1* larvae relative to WT at $p < 0.05$. Metabolites in red produce an MS/MS daughter ion with *m/z* 72.993. Data represent five biologically independent experiments and bars means ± standard deviation. **c,** Representative HPLC-MS (negative ion) EICs and MS/MS spectra for most abundant differential metabolites in **b**, bemeth#3 (**11**) and bemeth#2 (**12**). **d,** Overview of synthetic scheme to afford bemeth#2 (see Methods for details). **e,** Comparison of HPLC-MS (negative ion) EICs for synthetic diastereomers of bemeth#2 (**12**) and the corresponding metabolites in *exo*-metabolome extracts from WT and *hacl-1* larvae.

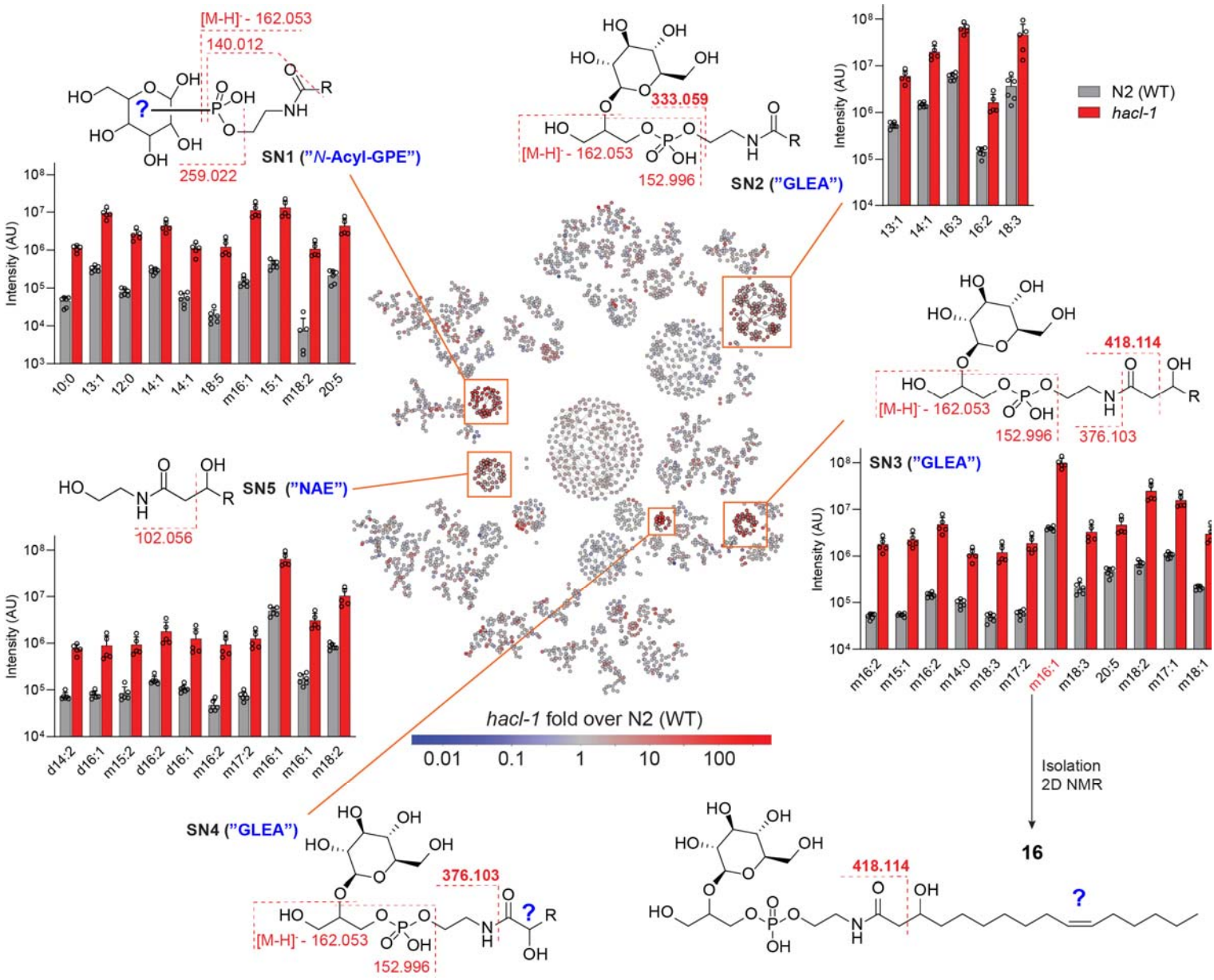

Figure 4. MS/MS network comparing *exo*-metabolomes of *hacl-1* and WT adults. Proposed structures and major fragmentation reactions are shown for five subnetworks (SN1 – SN5, orange boxes). Example compounds in the bar graphs are at least 10-fold enriched in *hacl-1* mutants relative to WT and satisfy mean intensity criteria (10^6 for SN1, SN2, SN3; $5*10^5$ for SN5). R represents an acyl group with N carbons and n degrees of unsaturation (N:n), preceded by *m* or *d* for *m*ono- or *d*i-oxygenated. The structure of the most abundant metabolite in SN3, GLEA-m16:1 (**16**), was characterized via 2D NMR spectroscopy. For compounds from SN4, see Supplementary Figure 9. Data represent six (WT) or five (*hacl-1*) samples from three biologically independent experiments and bars means ± standard deviation.

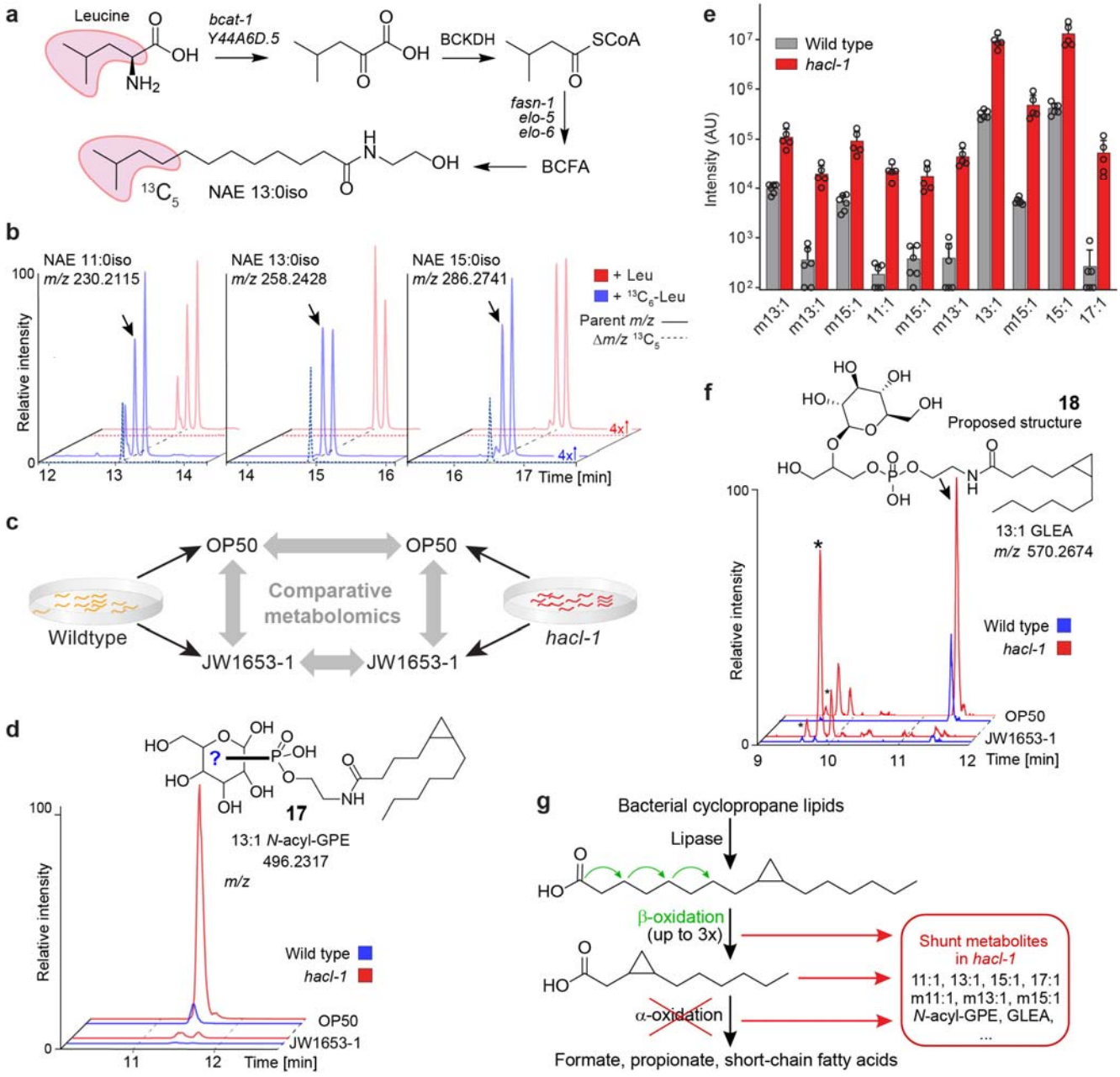

Figure 5. Cyclopropane-containing glycolipids are enriched in *hacl-1* mutants. **a,** Leucine metabolism feeds into branched-chain fatty acid (BCFA) biosynthesis in *C. elegans*. **b,** Pairwise analysis of Leu or $^{13}C_6$-Leu-supplemented worms using the *Label Finder* revealed $^{13}C_5$-enriched NAEs derived from BCFAs. Shown are representative HPLC-MS (ESI+) EICs and dotted lines represent incorporation of $^{13}C_5$ ($\Delta m/z$, 5.0167), as visualized using Metaboseek *Mass Shifts.* **c,** Study design for comparative metabolomics of WT and *hacl-1* worms fed either *E. coli* OP50 or cyclopropane fatty acid-deficient *E. coli* JW1653-1. **d**, Representative HPLC-MS (ESI-) EIC for 496.2317, corresponding to cyclopropane-containing *N*-acyl GPE 13:1 (**17**). Shown structure was proposed based on MS/MS fragmentation and absence in JW1653-1. **e**, Quantification of

749 *N*-acyl GPEs that were absent from worms fed JW1653-1. Data represent six (WT) or five (*hacl-*
750 *1*) samples from three biologically independent experiments and bars means ± SD. **f**,
751 Representative HPLC-MS (ESI-) EIC for *m/z* 570.2674, corresponding to cyclopropane-
752 containing GLEA 13:1 (**18**). Shown structure was proposed based on MS/MS fragmentation and
753 absence in JW1653-1. Asterisks (*) mark isobaric *hacl-1*-enriched features that are not
754 impacted by JW1653-1 diet. **g,** Proposed metabolism of bacterial 17:1 (or 19:1) cyclopropane
755 lipids. Three (or four) rounds of β-oxidation would produce an 11:1 cyclopropane fatty acid
756 unsuitable for further β-oxidation that could be a substrate for α- or ω-oxidation.

757